Tungsten and molybdenum dinitrogen complexes supported by a pentadentate tetrapodal phosphine ligand: comparative spectroscopic, electrochemical and reactivity studies

Jannik Junge, Sven Froitzheim, Tobias Engesser, Jan Krahmer, Christian Näther, Nicolas Le Poul, Felix Tuczek

Version submitted to Dalton Trans. on 15th Dec. 2021.

DOI: 10.1039/d1dt04212b

Tungsten and Molybdenum Dinitrogen Complexes Supported by a Pentadentate Tetrapodal Phosphine Ligand: Comparative Spectroscopic, Electrochemical and Reactivity Studies

Jannik Junge[†a], Sven Froitzheim[†a], Tobias A. Engesser[a], Jan Krahmer[a], Christian Näther[a], Nicolas Le Poul*[b], Felix Tuczek*[a]

[a]Institut für Anorganische Chemie, CAU Kiel, Max-Eyth-Str. 2, 24118 Kiel, Germany. E-mail: ftuczek@ac.uni-kiel.de
[b]Laboratoire de Chimie, Électrochimie Moléculaires et Chimie Analytique (UMR CNRS 6521), Université de Bretagne Occidentale, 6 Avenue Le Gorgeu, 29238 Brest, France. E-mail: lepoul@univ-brest.fr

The tungsten dinitrogen complex [W(N$_2$)(P$^{Me}_2$PP$^{Ph}_2$)] (2) is synthesized and characterized by X-ray diffraction as well as IR and NMR spectroscopies, showing strong analogies to its molybdenum analogue [Mo(N$_2$)(P$^{Me}_2$PP$^{Ph}_2$)] (1). Whereas cyclic voltammetry studies indicate very similar redox potentials, detailed electrochemical and IR-spectroelectrochemical investigations reveal characteristic differences between 1 and 2 upon electrochemical oxidation in THF. Protonation of 2 with HBAr^F leads to the hydrazido(2-) derivative 3 which is spectroscopically characterized as well. In the presence of SmI$_2$/H$_2$O slightly overstoichiometric conversion of N$_2$ to ammonia (2.75 eq.s) is observed. Although this is far below the activity of the Mo-complex 1, it renders 2 the first W complex to produce more than 2 equivalents of NH$_3$ from N$_2$ under catalytic conditions.

Introduction

The conversion of dinitrogen to ammonia under ambient conditions is one of the most challenging tasks of bioinorganic chemistry.[1] In nature, microorganisms which contain the enzyme nitrogenase perform this reaction.[2] In industry, ammonia is produced with the Haber-Bosch process, involving drastic conditions.[3] The activation of the highly inert dinitrogen molecule and the catalytic N_2-to-NH_3 conversion by transition metal complexes have been subject of research for decades. While Allen and Senoff succeeded in synthesizing the first dinitrogen complex in 1965,[4] the groups of Chatt and Hidai demonstrated the generation of ammonia from molybdenum and tungsten bis(dinitrogen) complexes with up to 90 % yield.[5] Later on, Pickett and Talarmin were able to electrochemically generate 0.73 equivalents of ammonia in a cyclic process.[6] The first truly catalytic system was developed by Schrock *et al.* in 2003 based on a molybdenum triamidoamine complex.[7,8] Using molybdenum complexes supported by different pincer ligands along with various protonating and reducing agents Nishibayashi *et al.* could gradually increase the amount of ammonia.[9] The best results were obtained with SmI_2 and H_2O, employing a Mo(III) complex with a PCP-pincer ligand as precatalyst.[10]

Whereas molybdenum complexes have been highly successful regarding the catalytic conversion of N_2 to ammonia, no catalytically active tungsten complex has so far been reported.[7,11,12] Sometimes, tungsten analogues of molybdenum catalysts could not be prepared,[11] and even if the former were synthetically accessible, they so far always turned out to be catalytically inactive.[12] To the best of our knowledge, no compelling reason for this striking difference in reactivity has been given. For the tungsten triamidoamine system, it was speculated that, due to a more negative reduction potential of the W(I)-NH_3 intermediate as compared to its Mo(I) analogue, the starting dinitrogen complex could not be reformed with the employed reductant.[12] On the other hand, oxidation potentials for the corresponding Mo(0) and W(0) dinitrogen complexes turned out to be quite similar.[12] In 2016, our working group presented the molybdenum dinitrogen complex [Mo(N$_2$)(P$^{Me}_2$PP$^{Ph}_2$)] (**1**) supported by the pentadentate tetrapodal (pentaPod) ligand P$^{Me}_2$PP$^{Ph}_2$ (Scheme 1).[13] This system was, with 26 equivalents of NH_3, the first catalytic single-coordination site complex which follows the mechanism of the so called Chatt cycle, showing that the pentaPod ligand eliminates the problems of the latter; i.e., the loss of 50 % of the catalyst each cycle and the dissociation of the M-P bond which can occur when ligands with lower denticity are used.[14]

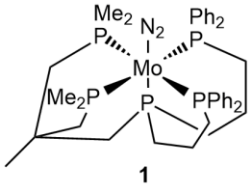

1

Scheme 1. Molybdenum dinitrogen complex [Mo(N$_2$)(P$^{Me}_2$PP$^{Ph}_2$)] (**1**) supported by a tetrapodal pentadentate phosphine ligand.[13]

Despite the fact that this Mo(0) dinitrogen complex and its hydrazido(2-) derivative were found to be active catalysts, DFT calculations of the N-H bond dissociation free energy (BDFE) of the respective diazenido complex in the framework of a PCET mechanism indicated that the reaction path could also involve a cationic, mononuclear $Mo^{I}(N_2)^{+}$ intermediate.[14]
In order to gain more information about the differing behaviour of molybdenum and tungsten complexes towards catalytic N_2-to-NH_3 conversion, we herein present the tungsten dinitrogen complex $[W(N_2)(P^{Me}{}_2PP^{Ph}{}_2)]$ (**2**) supported by the above-mentioned pentaPod ligand for comparative investigations with its molybdenum analogue (**1**). Notably, with $[W(N_2)(PMe_3)_5]$, there has been only one example of a tungsten dinitrogen complex with a pentaphosphine environment so far.[15] Moreover, in order to determine the role of $M^{I}(N_2)^{+}$ complexes during the catalytic process, the electrochemical properties of the $M^{0}(N_2)$ pentaPod complexes (M = Mo (**1**) and W (**2**)) as well as the stabilities of their one-electron oxidized $M^{I}(N_2)^{+}$ counterparts are investigated. To this end, cyclic voltammetry investigations combined with in-situ IR-spectroelectrochemical experiments are conducted on **1** and **2**. Finally, the reactivities of the W complex **2** towards acids and the reduction of N_2 to ammonia using SmI_2/H_2O are investigated and compared with results obtained on the analogous molybdenum system **1**. The implications of the experimental findings regarding the role of the two metal centers in synthetic nitrogen fixation and the corresponding mechanistic pathways are discussed.

Results and Discussion

1. Synthesis and characterization of the W-N_2 complex

The synthesis and characterization of the $Mo(N_2)$ complex $[Mo(N_2)(P^{Me}{}_2PP^{Ph}{}_2)]$ (**1**) was described before.[13,14] The analogous tungsten(0) dinitrogen complex **2** was synthesized by sodium amalgam reduction of $[WCl_3(\kappa^3\text{-}P_2{}^{Me}PP_2{}^{Ph})]$ (for EPR and IR data see Figures S1, S2 and Table S1). This W(III) complex with a precoordinated pentaPod ligand was in turn obtained through reaction of $P^{Me}{}_2PP^{Ph}{}_2$ with $[WCl_4(PMePh_2)]$ in toluene (Scheme 2), whereby the released methyldiphenylphosphine acts as reducing agent.

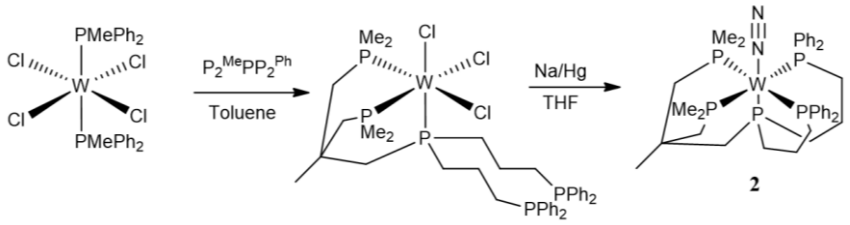

Scheme 2. Synthesis of $[W(N_2)(P^{Me}{}_2PP^{Ph}{}_2)]$ (**2**).

In agreement with $Mo(N_2)$ complexes exhibiting a topologically related pentaphosphine coordination,[13,16] the ^{31}P NMR spectrum of **2** exhibits an AA'MXX' pattern (Figure 1b, c and Figures S3-S7). In order to obtain information about the bonding situation between the coordinated N_2 ligand, the tungsten atom and the phosphine ligands, the ^{15}N-labelled complex was synthesized and the couplings were analyzed by NMR (Figure 1a). ^{183}W satellites were detected with $^{1}J_{W\text{-}P}$ coupling constants between 254 Hz and 315 Hz, similar to the values found in the literature for a comparable complex.[15]

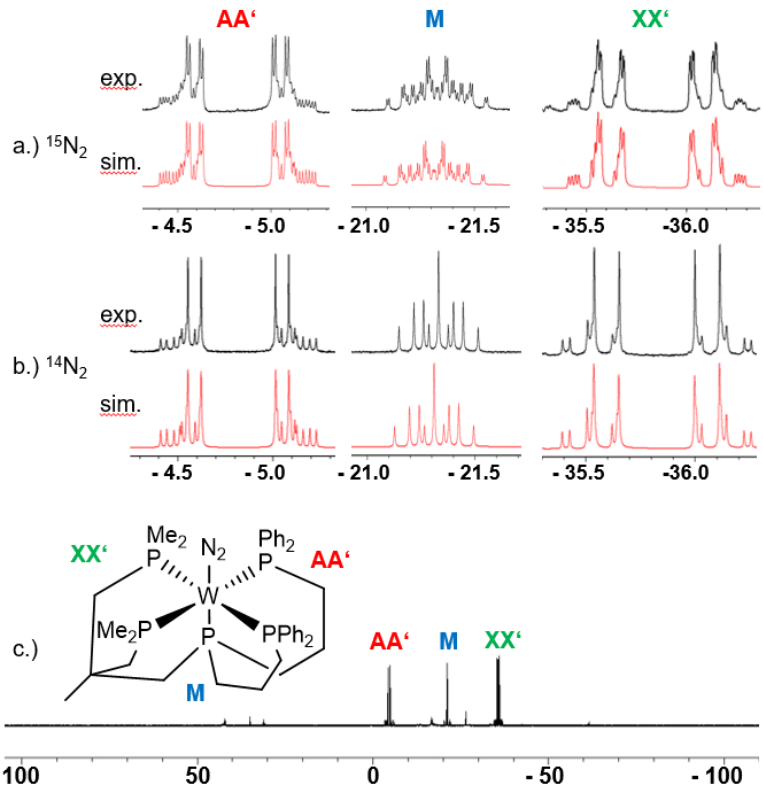

Figure 1. Experimental and simulated $^{31}P\{^1H\}$ NMR spectra of **$^{15}N_2$-2** (a) and **2** (b). c.) Overall spectrum of **2** in tetrahydrofuran-d_8 at 300 K. The signals were assigned based on the ^1H-^{31}P-HMBC NMR spectrum (Figure S6).

Comparison between the ^{31}P NMR spectrum of the tungsten complex with the molybdenum analogue showed a high-field shift of the tungsten signals between -30 and -34 ppm. In addition, the *cis* coupling constants in the tungsten complex all are about 10 Hz smaller than in the molybdenum complex whereas the *trans* coupling constants of both complexes are about equal. Similar trends have been described in the literature.[17] The ^{15}N-^{15}N and the ^{15}N-^{31}P coupling constants differ by less than 1 Hz between **1** and **2** (see Table S2). IR spectroscopy of crystalline **2** shows an N-N stretching vibration at 1901 cm^{-1} which shifts to 1840 cm^{-1} for the ^{15}N isotope labelled complex (**^{15}N-2**; for an analysis of the IR spectra see Table S3). Notably, this frequency is lower than ν(NN) determined for the Mo analogue **1** (1929 cm^{-1}).[13]

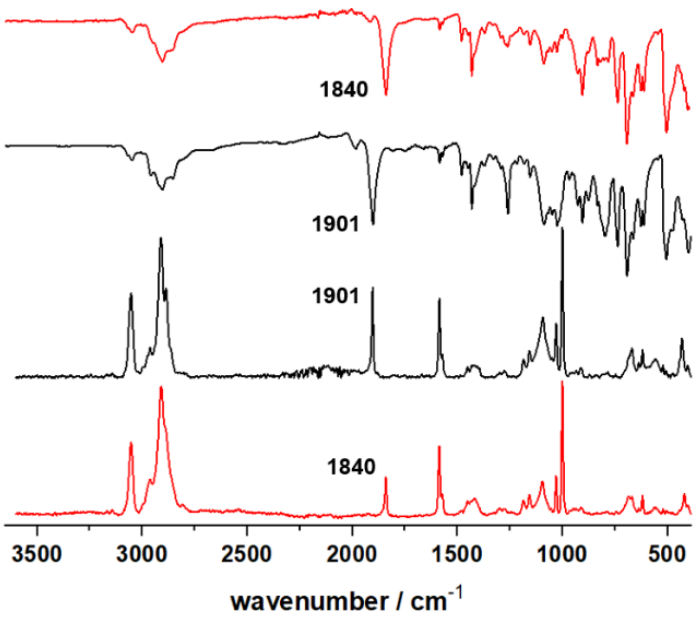

Figure 2. IR and Raman spectra of **2** (black) and **$^{15}N_2$-2** (red).

By layering a benzene solution with *n*-pentane, single crystals of **2** could be obtained. X-ray analysis shows a molecular structure with a pentaphosphine environment, thus confirming the results of ^{31}P NMR spectroscopy (Figure 3, for crystal data see ESI Figure S8 and Table S4). Comparison with the molybdenum analogue shows similar metal-ligand bond lengths which agrees with the literature and can be explained with almost the same ionic radius (Table S5).[15,18] The N_α-N_β bond distance is also practically identical to that of the Mo complex (Table S6).

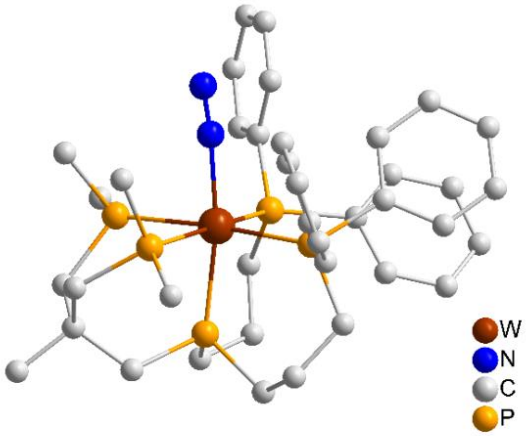

Figure 3. Single-crystal structure of [W(N_2)($P^{Me}_2PP^{Ph}_2$)] (**2**). The hydrogen atoms have been omitted for clarity.

Table 1. Chemical shift and coupling constants of [Mo(N_2)($P^{Me}_2PP^{Ph}_2$)] (**1**),[13] [W(N_2)($P^{Me}_2PP^{Ph}_2$)] (**2**), Mo(NNH_2)($P^{Me}_2PP^{Ph}_2$)]$^{2+}$[14] and [W(NNH_2)($P^{Me}_2PP^{Ph}_2$)]$^{2+}$ (**3**). AA´, M and XX´ refer to Figure 1.

Complex	δ/ppm			*J*/Hz						Ref.
	M	AA'	XX'	$J_{MA/MA'}$	$J_{MX/MX'}$	$J_{AA'}$	$J_{AX'/A'X'}$	$J_{AX/A'X'}$	$J_{XX'}$	
[**W**(N_2)] (**2**)	-21.3	-4.8	-35.8	11.2	18.5	4.5	85.7	-11.1	17.4	This
[**Mo**(N_2)] (**1**)	12.4	25.5	-3.7	20.4	28.7	14.7	83.4	-19.8	27.4	study[13]
Δ	-33.7	-30.3	-32.1	-9.2	-10.2	-10.2	2.3	8.7	-10.0	
[**W**(NNH_2)]$^{2+}$(**3**)	-48.5	-15.9	-45.8	28.2	31.3	6.3	53.9	-12.2	16.1	This study
[**Mo**(NNH_2)]$^{2+}$	-32.3	11.4	-14.7	32.7	39.1	16.5	56.5	-20.8	26.9	[13]
Δ	-16.2	-27.3	-31.1	-4.5	-7.8	-10.2	-2.6	8.6	-10.8	

Mo = Mo($P^{Me}_2PP^{Ph}_2$); **W** = W($P^{Me}_2PP^{Ph}_2$);

The ligand sphere of **2** corresponds to a distorted octahedron with the P_{ax}-W-N_α angle (170.65(9)°) significantly deviating from linearity. Notably, the W-P_{ax} bond length (2.3828(1) Å) is shorter than the average W-P_{eq} bond length (2.4375 Å, Figure 3). In the other known tungsten dinitrogen complex with a pentaphosphine ligation, [W(N_2)(PMe_3)$_5$],[15] the M-P bond length of the phosphine in *trans* position to the N_2 ligand is longer than the M-P bond lengths of the equatorial phosphines.
The shortening of the *trans* M-P bond length thus appears to be due the topology of the pentaPod ligand. As already noticed for the Mo-complex **1**, this does not cause an elongation of the M-N_2 bond (W-N_α = 2.020(5) Å, Mo-N_α = 2.033(5) Å), indicating that the *trans*-phosphine, apart from being a strong σ–donor, also exhibits a significant degree of π-backbonding.

2. Electro- and spectroelectrochemical studies

Cyclic voltammetry and IR spectroelectrochemistry were carried out in order to determine the redox potentials and characterize the species formed upon oxidation of the tungsten(0) and molybdenum(0) pentapod-N_2 complexes **2** and **1**, respectively. The studies were performed in dry THF/$NaBPh_4$ (20 mM) under argon atmosphere in a glovebox. Since both complexes are extremely sensitive, their stability in THF/$NaBPh_4$ was first checked by IR spectroscopy. In that electrolyte, no change in the N_2 stretching signal could be observed over 6 days, ensuring that the electrochemical results can in fact be assigned to the tungsten and molybdenum N_2 species.

Cyclic voltammetry at a Pt electrode was first performed at different scan rates (0.02 V s^{-1} < *v* < 5 V s^{-1}) for the tungsten complex **2**. In reduction, no cathodic peak could be observed at potentials down to the limit where electrolyte reduction occurs (-2.9 V *vs.* Fc^+/Fc). On the anodic side, for low-to-moderate scan rates (0.02 V s^{-1} < *v* < 0.2 V s^{-1}), two main systems were detected upon oxidation, the first one being reversible at $E_{1/2}(1)$ = −1.16 V while the other appeared as irreversible at ca. $E_{pa}(2)$ = −0.25 V *vs.* Fc^+/Fc (Figure 4-A). When increasing *v* up to 5 V s^{-1}, the second system displayed more reversibility (Figure 4-B) whereas the first remained fully reversible, hence suggesting that a moderately fast (ms) chemical process follows the second oxidation. Linear plots of the anodic peak current i_{pa} *vs.* $v^{1/2}$ (Figure S9-A) not only pointed to a diffusion-limited process for the first oxidation, but also allowed the determination of the number of electrons from the Randles-Sevcik equation[19], applying a diffusion coefficient *D* = 9.5·10^{-6} cm^2 s^{-1} determined by ^{1}H NMR DOSY for the W(N_2) complex **2** (see ESI Figure S10). This treatment indicated that the latter process is monoelectronic. In addition, the anodic peak current function (i_{pa} $v^{-1/2}$) was plotted against *v* for both oxidation processes. As clearly shown in Figure 4-C, the value of $i_{pa}(1)$ $v^{-1/2}$ remains relatively constant whatever *v* for the first oxidation, as expected for a simple electron transfer. However, for the second oxidation process, a significant increase of $i_{pa}(2)$ $v^{-1/2}$ is detected for *v* < 0.2 V s^{-1}. This is consistent with a multiple electron transfer that is kinetically limited by a chemical process, as classically found for an ECE mechanism (E = Electrochemical, C = Chemical).[19] The chemical process is likely here a N_2-solvent ligand exchange at the W(II) redox state,[20] which is followed by an electrochemical oxidation, generating a W(III) species (Scheme 3).

In order to characterize the species generated at the first and second oxidation processes, IR-spectroelectrochemical studies were performed for [W(N_2)($P^{Me}_2PP^{Ph}_2$)] (**2**, see experimental part for details). As shown in Figure 4-D, oxidation at $E_{pa}(1)$ caused disappearance of the N_2 band at 1915 cm^{-1} concomitant with the emergence of a new band at 1951 cm^{-1}. Switching back the potential to its initial value allowed complete recovery of the original infrared spectrum. This demonstrates the full reversibility of the process, in agreement with low-scan-rate CV studies. Upon further oxidation at $E_{pa}(2)$, the newly-formed band at 1951 cm^{-1} disappeared and could only be obtained upon back-reduction to the initial potential (Figure S9-D).
Aiming at determining the role of the metal in the described redox processes, we carried out the same experiments for [Mo(N_2)($P^{Me}_2PP^{Ph}_2$)] (**1**). CV studies revealed several differences compared to the W-N_2 complex. For instance, the first oxidation process at $E_{1/2}(1)$ was found to be not fully reversible at low scan rate (*v* < 0.1 V s^{-1}). Moreover, a supplementary irreversible anodic peak at $E_{pa}(3)$ (ca. −0.7 V *vs.* Fc^+/Fc) was detected for *v* < 0.5 V s^{-1} (Figure 5-A). Further oxidation at $E_{pa}(2)$ was also accompanied by a supplementary oxidation peak at $E_{pa}(4)$ which disappeared at high scan rate (Figure 5-B). At last and conversely to complex **2**, the Mo complex displayed no sign of reversibility for the second reduction process at $E_{pa}(2)$ for high values of *v* (Figure 5-B and Figure S-9B).

Spectroelectrochemical studies performed with the Mo-N_2 complex **1** also revealed some differences to its W congener **2**. While oxidation at $E_{pa}(1)$ led to disappearance of the N_2 stretching band at 1942 cm^{-1}, no new IR-detectable species could be detected in the 1800 – 2100 cm^{-1} frequency range (Figure 5-C). Moreover, upon back reduction, the initial spectrum could only be partially recovered. Interestingly, analysis at lower frequencies (1400 to 1700 cm^{-1}) displayed further spectral changes upon electrochemical oxidation (Figure 5-D). Pushing the potential until $E_{pa}(2)$ induced even larger modification of the spectra in this frequency region. Returning to the initial potential value partially restored the N_2 stretching band at 1942 cm^{-1} (Figure 5--D). Notably, the changes in the 1400 to 1700 cm^{-1} frequency range were not observed for the tungsten complex upon oxidation at $E_{pa}(2)$ (Figure S9-D).

Altogether, these electrochemical and spectroelectrochemical investigations essentially revealed two results. First, they clearly show that monoelectronic oxidation of the neutral W and Mo dinitrogen complexes occurs at almost the same $E_{1/2}(1)$ value (−1.16 V and −1.13 V *vs.* Fc^+/Fc, respectively). This result is reasonable on the basis of experimental data obtained from NMR and IR spectroscopies as well as X-ray diffraction (*vide infra*), which have shown minor differences between the two neutral Mo and W complexes in solution and in the solid state. It is also in line with electrochemical investigations reported on Mo and W bis-N_2 complexes supported by $P^{Ph}N^{Me}P^{Ph}$ ligands, exhibiting a difference of only 20 mV for the first oxidation potential.[21] Hence, our results suggest that the structural properties of the W and Mo mono-oxidized dinitrogen species are very similar.
The second information which can be taken from electrochemistry and spectroelectrochemistry is that, although $W^I(N_2)^+$ and $Mo^I(N_2)^+$ pentaPod complexes can be reduced at similar potential values, they display very different stabilities in THF (cf. Scheme 3): whereas the mono-oxidized tungsten N_2 species seems to be highly stable, yielding back the neutral N_2 complex upon reduction, spectroelectrochemistry suggests that its Mo analogue evolves rapidly (sec) towards a new Mo^I species, probably a $Mo^I(thf)^+$ complex. Likewise, the $W^{II}(N_2)^{2+}$ species appears at the second oxidation process as fairly unstable (msec) and may exchange its N_2 ligand by a THF ligand. Upon back reduction, N_2 re-binds to the metal center since the N_2 stretching band is detected. In the case of the molybdenum complex, oxidation beyond $E_{pa}(1)$ leads to a more complicated situation and probably induces N_2-THF ligand exchange. The anodic peak at $E_{pa}(3)$ may be thus ascribed to the oxidation of $Mo^I(thf)^+$ species.

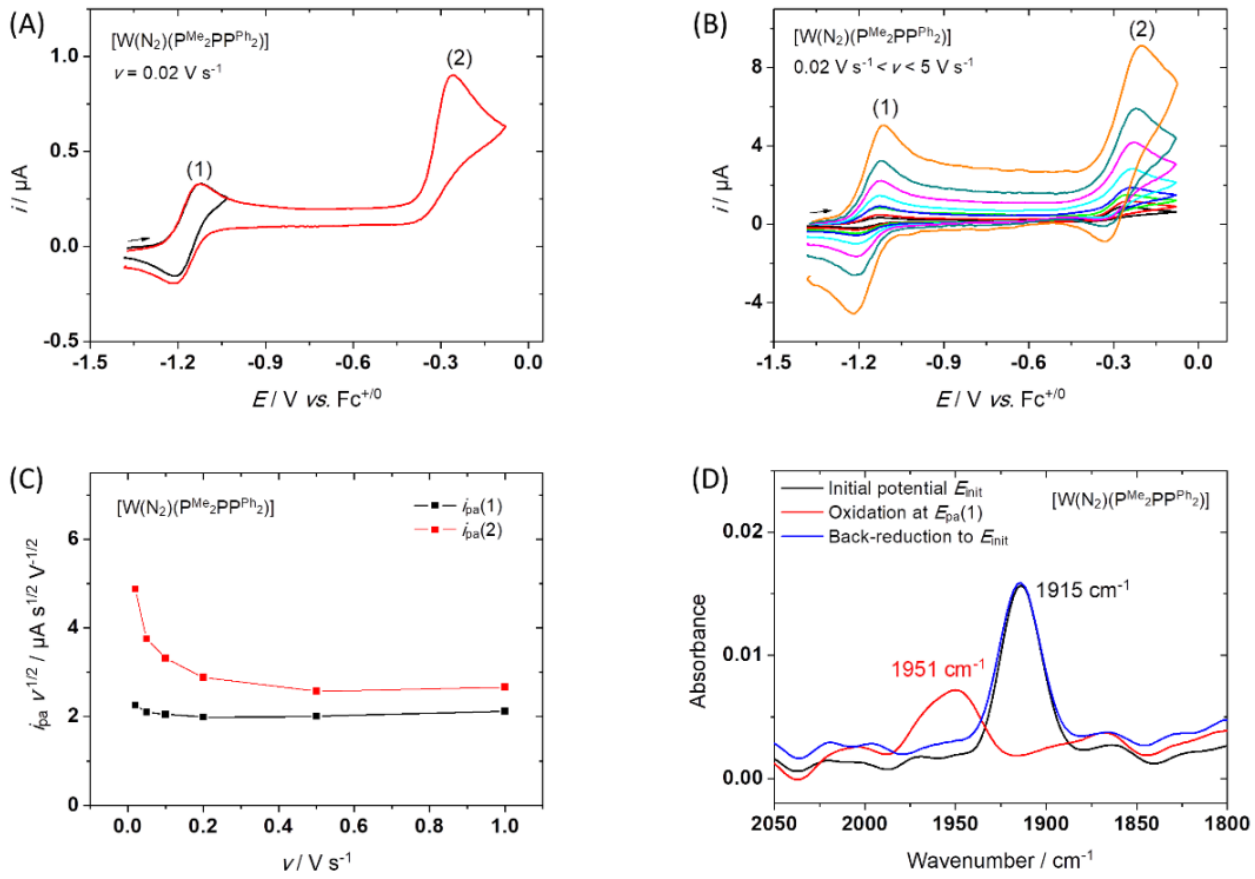

Figure 4. CVs (*E* / V *vs.* Fc^{+}/Fc) at a Pt working electrode (diam. 1 mm) of $[W(N_2)(P^{Me}{}_2PP^{Ph}{}_2)]$ (0.4 mM) in THF/$NaBPh_4$ 0.02 M (A) at v = 0.02 V s^{-1} and (B) for v = 0.02 V s^{-1} (black), 0.05 V s^{-1} (red), 0.1 V s^{-1} (green), 0.2 V s^{-1} (blue), 0.5 V s^{-1} (cyan), 1 V s^{-1} (pink), 2 V s^{-1} (olive) and 5 V s^{-1} (orange); The numbers (1) and (2) on the graphics are related to the redox systems, see details in text. (C) Plots of $i_{pa}(1)\ v^{-1/2}$ (black squares) and $i_{pa}(2)\ v^{-1/2}$ (red squares) against v from CV data in (B); (D) Infrared spectra of $[W(N_2)(P^{Me}{}_2PP^{Ph}{}_2)]$ (15 mM) in THF/$NaBPh_4$ 20 mM recorded during *in-situ* spectroelectrochemical measurements before (black) and after oxidation at $E_{pa}(1)$ (red), then returning back to the initial potential (blue).

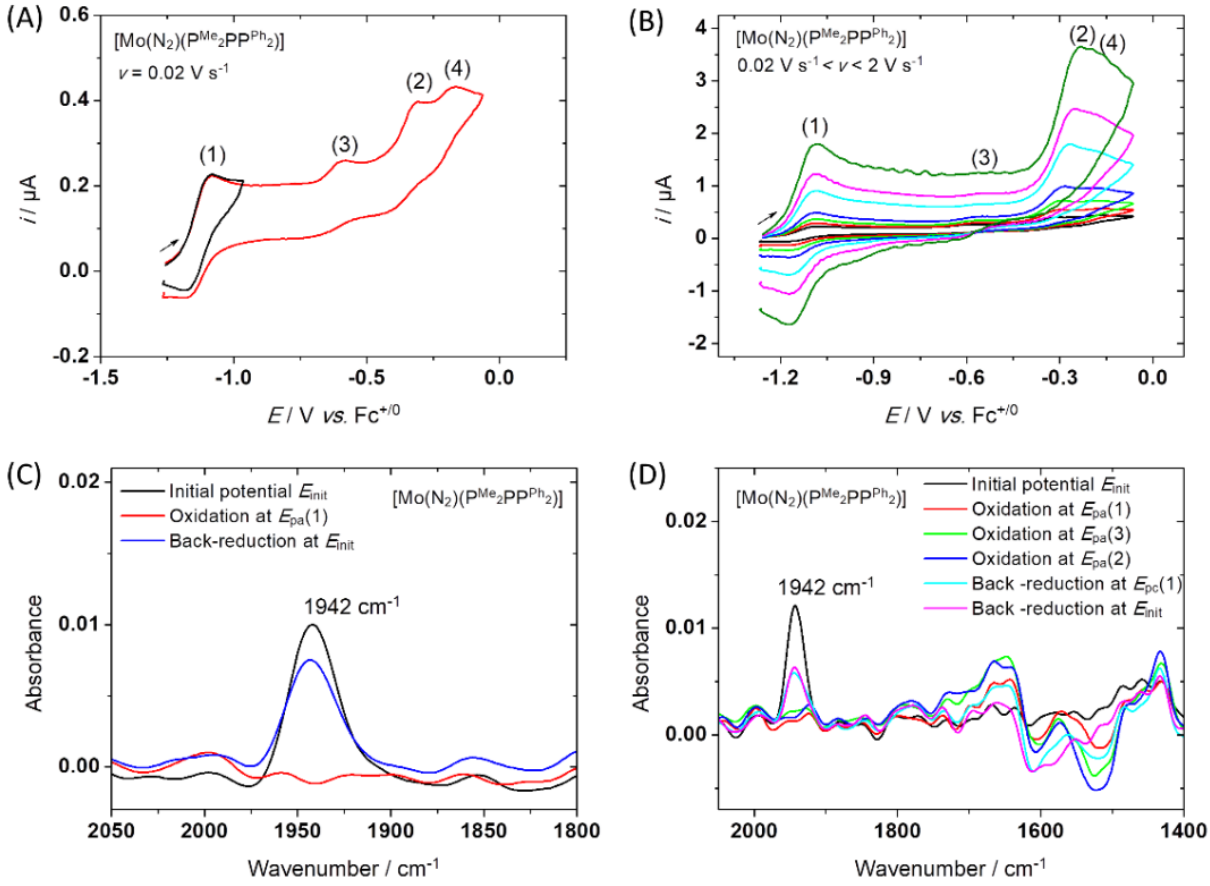

Figure 5. CVs (*E* / V *vs.* Fc^+/Fc) at a Pt working electrode (diam. 1 mm) of $[Mo(N_2)(P^{Me}{}_2PP^{Ph}{}_2)]$ (0.4 mM) in THF/$NaBPh_4$ 0.02 M (A) at v = 0.02 V s^{-1} and (B) for v = 0.02 V s^{-1} (black), 0.05 V s^{-1} (red), 0.1 V s^{-1} (green), 0.2 V s^{-1} (blue), 0.5 V s^{-1} (cyan), 1 V s^{-1} (pink) and 2 V s^{-1} (olive); The numbers (1), (2), (3) and (4) on the graphics are related to the redox systems, see details in text. (C) Infrared spectra of $[Mo(N_2)(P^{Me}{}_2PP^{Ph}{}_2)]$ (15 mM) in THF/$NaBPh_4$ 20 mM recorded during *in-situ* spectroelectrochemical measurements before (black) and after oxidation at $E_{pa}(1)$ (red), then returning back to the initial potential (blue); (D) The same as (C) except that oxidation at $E_{pa}(1)$ (red) is followed by oxidation at $E_{pa}(3)$ (green), $E_{pa}(2)$ (blue), then returning back to the $E_{pa}(1)$ (cyan) and finally the initial potential (magenta).

Table 3. Electrochemical data for $[LM^{I/0}]$ dinitrogen species.

Complex	$E_{1/2}$ / V *vs.* Fc^+/Fc	Conditions	Ref.
$[W(N_2)(P^{Me}{}_2PP^{Ph}{}_2)]$ (**2**)	−1.16	THF/ $NaBPh_4$	This work
$[Mo(N_2)(P^{Me}{}_2PP^{Ph}{}_2)]$ (**1**)	−1.13	THF/ $NaBPh_4$	This work
$[Mo(N_2)(HIPTNCH_2CH_2)_3N]$	−0.42[a]	THF/NBu_4PF_6	[22]
	−0.66	PhF/ $NBu_4[B(C_6F_5)_4]$	
trans-$[Mo(depe)_2(N_2)_2]$	−1.01	THF/Pyr_4FAP	[23]
	−0.99[b]	THF/NBu_4BF_4	[24]
trans-$[W(dppe)_2(N_2)_2]$	−0.82	THF/$NBu_4[B(C_6F_5)_4]$	[21]
trans-$[W(dppe)(dppp)(N_2)_2]$	−0.79	THF/$NBu_4[B(C_6F_5)_4]$	[21]
$(\mu\text{-}N_2)[Mo(N[t\text{-}Bu]Ar)_3]_2$	−1.46[c]	THF/$NBu_4[B(C_6F_5)_4]$	[25]
	−0.32[d]		
$(\mu\text{-}N_2)[W(t\text{-}BuC_6H_4N_3N)]_2$	−1.64[c]	THF/NBu_4PF_6	[26]
	−0.75[d]		
$(\mu\text{-}N_2)[Mo(t\text{-}BuC_6H_4N_3N)]_2$	−0.98[c]	THF/NBu_4PF_6	[26]
	−0.04[a,d]		
$(\mu\text{-}N_2)[Mo(C_6F_5N_3N)]_2$	−0.43[c,e]	THF/NBu_4PF_6	[26]
$(\mu\text{-}N_2)[MoCl(PNP)_2]_2$	−1.14[c]	THF/NBu_4PF_6	[27]
	−0.64[d]		

[a]Irreversible peak at v = 0.1 V s^{-1}; [b]Experimentally measured at $E_{1/2}$ = −0.43 V *vs.* SCE; [c]Mo^IMo^0 redox couple; [d]Mo^IMo^I redox couple. [e]According to the authors, the second oxidation is irreversible and appears at E > −0.3 V *vs.* Fc^+/Fc ; [f]Experimentally measured at $E_{1/2}$ = −0.16 V *vs.* SCE.

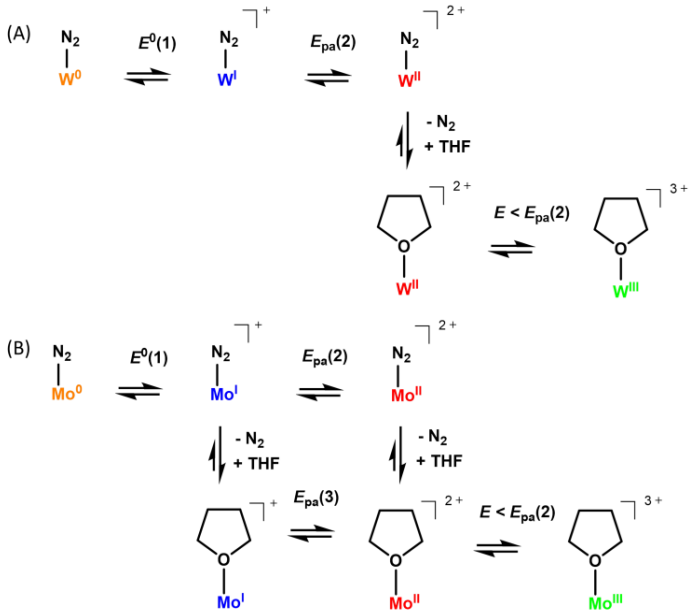

Scheme 3. Proposed mechanism for the oxidation processes of the tungsten (A) and molybdenum (B) pentaPod N_2 complexes.

At last, comparison with redox data reported for other dinitrogen Mo and W complexes offers interesting information (see Table). For instance, the mononuclear [Mo(N_2)(HIPTN_3N)] complex reported by Schrock *et al.*[22] displays a significantly higher oxidation potential than [Mo(N_2)($P^{Me}_2PP^{Ph}_2$)] (**1**) for the $Mo^{I/0}$ process in THF (–0.42 V against –1.16 V, respectively, Table). This difference may be explained by the different oxidation states of Mo. Furthermore, the mono-oxidation process is not reversible in THF for Schrock's complex, contrary to **1** and **2**. Another interesting comparison can be made with mononuclear *trans*-bis-N_2 W and Mo complexes. As shown in Table, oxidation potential values are clearly more positive than those of W and Mo pentaPod complexes by 150-370 mV, likely resulting from replacement of one dinitrogen ligand by a P-donor. In some cases, such as for *trans*-[Mo(dppe)$_2$(N_2)$_2$], the CV reversibility for the first oxidation was found to be dependent on the experimental conditions. Whereas Chatt *et al.* described a reversible system in THF/NBu_4BF_4 for the first oxidation process,[24] Elson reported an irreversible anodic peak at room temperature when using a THF/MeOH (26% v:v) mixture with LiCl or $LiClO_4$ as supporting electrolyte.[20] In the latter case, a *trans*-[Mo^{I}(dppe)$_2$(MeOH)$_2$]$^+$ species was characterized resulting from the release of N_2 according to a dissociative pathway. On the other hand, for *trans*-[Mo(depe)$_2$(N_2)$_2$],[23] longer timescale yielded N≡N bond cleavage and Mo^{IV} nitride formation, differently to the complex **1**.
Finally, Table collects data for dinuclear μ-N_2 Mo and W complexes which were shown to undergo metal-based mono-oxidation at redox potential values between –0.98 V and –1.64 V. For most of these bimetallic complexes, the first oxidation was reversible, consistent with the formation of a stable mono-oxidized mixed-valent μ-N_2 species.

3. Reactivity of Mo and W complexes towards acids and SmI_2/H_2O

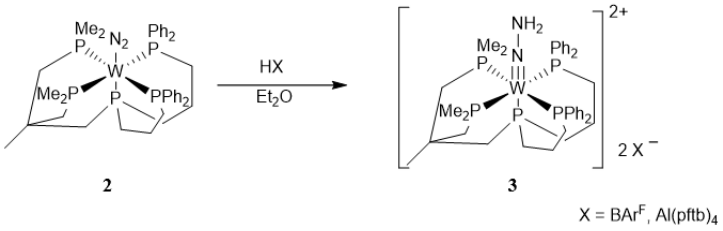

Scheme 4. Protonation of [W(N_2)($P^{Me}_2PP^{Ph}_2$)] (**2**) to [W(NNH_2)($P^{Me}_2PP^{Ph}_2$)]X_2 (X = BAr^F, Al(pftb)$_4$) (**3**).

In case of the molybdenum pentaPod complex [Mo(N_2)($P^{Me}_2PP^{Ph}_2$)] (**1**) the corresponding hydrazido(2-) complex could be generated by addition of Brookhart's acid ($HBAr^F$, [H(OEt_2)$_2$][BAr^F], 2.5 eq.s). Notably, this complex also exhibited catalytic activity towards ammonia generation, indicating that it is an intermediate of the catalytic cycle.[14] Treatment of the tungsten dinitrogen complex **2** with 2.5 eq.s of $HBAr^F$ was similarly found to generate the corresponding hydrazido(2-) complex **3-BAr^F** (Scheme 4; for IR data see ESI Figure S11 and Table S7). Using smaller amounts of acid does not lead to a pure product.
The ^{31}P NMR spectrum of **3-BAr^F** exhibits an AA'MXX' pattern (Figure 6, see Figures S12 to S17 for full NMR data), demonstrating retention of the pentaphosphine environment. However, all signals have undergone a high field shift compared to the dinitrogen

complex **2** (Figure 7), indicating an increased shielding of the P-donors in **3-BAr^F** which is attributed to an elongation of the metal-P bonds and a loss of π-donation to the metal center. The particularly large high-field shift of the M-signal upon protonation of the N_2-complex is due to the large *trans*-influence of the □-donating hydrazido(2-) ligand, weakening the W-P_{ax} bond. This analysis is supported by DFT calculations which show an increase of the W-P bond lengths upon going from **2** to **3**, with a larger elongation of the W-P_{ax} bond length in comparison to W-P_{eq} (Table S6). Notably, protonation of **2** with $[H(OEt_2)_2][Al(OC(CF_3)_3)_4]$ ($HAl(pftb)_4$) led to similar results (cf. Figure S18).

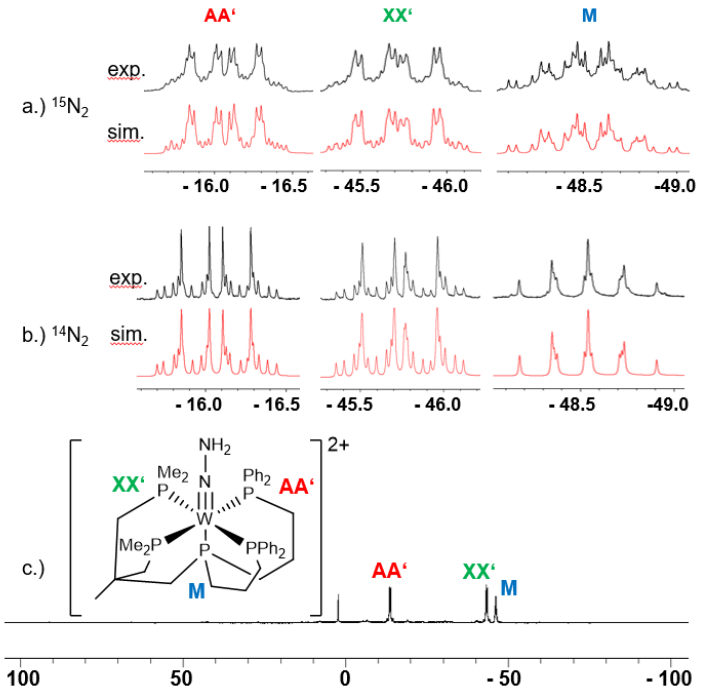

Figure 6. Experimental and simulated $^{31}P\{^1H\}$ NMR spectra of **$^{15}N_2$-3-BAr^F** (a) and **3-BAr^F** (b). c.) Overall spectrum of **3-BAr^F** in diethylether-d_{10}.

The ^{31}P-^{31}P coupling constants of the hydrazido(2-) complex **3-BAr^F** show some differences compared to the parent dinitrogen complex **2** (Table 1). While the *cis* couplings among the equatorial phosphines are almost unchanged (ΔJ = 1-2 Hz), the corresponding *trans* coupling gets smaller by about 30 Hz. On the other hand, the *cis* couplings of the equatorial phosphines with the axial P donor are increased by 17 and 13 Hz, respectively. Similar protonation-induced changes have been observed in the corresponding molybdenum system.[13,14] Comparison of the hydrazido(2-) complexes of tungsten and molybdenum show similar differences as for the dinitrogen complexes, except that the changes in the *cis* coupling constants between the equatorial phosphines and the axial P-donor are smaller than for the corresponding dinitrogen complexes. The ^1H-^{15}N, ^{15}N-^{15}N and ^{15}N-^{31}P coupling constants show nearly similar values, the corresponding values for the tungsten complexes always being slightly smaller than for their molybdenum counterparts (see Table S8 in ESI). Nevertheless, the ^1H-^{15}N coupling constant of **3-BAr^F** (92.0 Hz) is still larger than for a W-hydrazido(2-) complex supported by two bidentate ligands (80 Hz).[29] Analogous to the dinitrogen complexes, DFT calculations indicate that the bond lengths and bond angles for the molybdenum and tungsten hydrazido(2-) complexes are very similar (Table S6). Moreover, the calculated N-N bond lengths (~1.31 Å) correspond to those obtained for classic Chatt-type hydrazido(2-) complexes.[30]

In order to investigate a potential catalytic activity of the new tungsten complex, a 0.1 M solution of samarium diiodide and water was treated with a THF solution of **2** (2 µmol in 1 ml THF) under nitrogen. After the solution turned yellow the amount of produced ammonia was determined by the indophenol method.[28] In contrast to its molybdenum congener **1**, complex **2** just generated a slightly over-stoichiometric amount of ammonia (2.75 ± 0.23 eq., 5 % yield related to the reducing agent). Whereas a lack of catalytic activity regarding ammonia formation from N_2 is well known for tungsten systems (see above),[11,12] we note that **2** is the first W complex that is able to generate more than 2 equivalents of NH_3 in relation to the metal centre, showing that the originally coordinated dinitrogen is converted to ammonia. However, it appears that just a small fraction of the dinitrogen complex is regenerated, suggesting that most of the catalyst is converted to a different complex that is inactive towards nitrogen reduction.

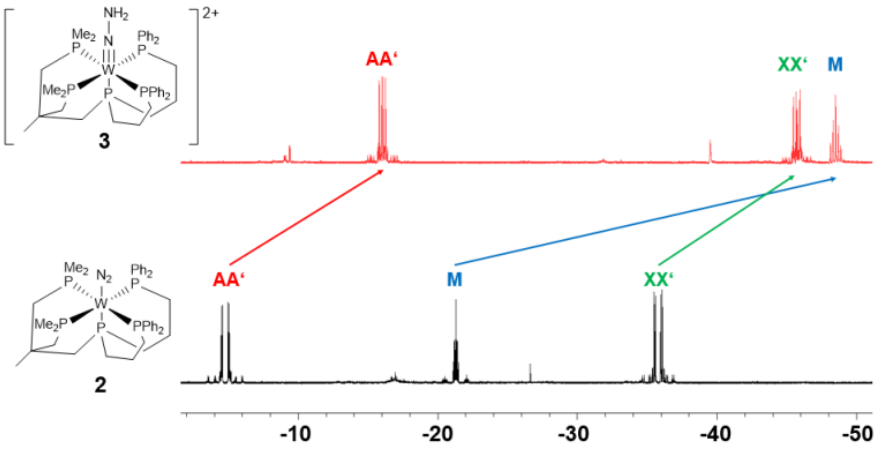

Figure 7. Comparison of the $^{31}P\{^{1}H\}$ NMR spectra of **2** (black) and **3-BAr^{F}** (red).

4. Summary and Conclusions

The tungsten dinitrogen complex [W(N$_2$)(P^{Me}$_2$PP^{Ph}$_2$)] (**2**) supported by a pentadentate tetrapodal phosphine ligand (P^{Me}$_2$PP^{Ph}$_2$) has been synthesized and characterized regarding its electronic structure and reactivity, allowing comparison with the analogous molybdenum complex [Mo(N$_2$)(P^{Me}$_2$PP^{Ph}$_2$)] (**1**). Reaction of [W(N$_2$)(P^{Me}$_2$PP^{Ph}$_2$)] (**2**) with samarium iodide/water was found to mediate a slightly overstoichiometric formation (2.75 ± 0.23 eq.) of NH$_3$ from N$_2$ which makes **2** the first tungsten complex generating more than 2 equivalents of ammonia from N$_2$. Notably, the analogous molybdenum complex **1** catalytically generates 25.7 eq. NH$_3$ from N$_2$.[14] This contrasting behaviour of tungsten *vs.* analogous molybdenum complexes regarding the catalytic conversion of N$_2$ to NH$_3$ is well known in the literature,[8,11] but not understood. With a ν_{NN} value of 1901 (**2**) vs. 1929 cm^{-1} (**1**) the activation of the N$_2$ ligand is higher in the W complex than in its Mo analogue, which therefore cannot be the reason for the differing behaviour. Apart from that, however, differences in structural parameters are small. Correspondingly, a single-crystal structure determination of **2** only showed minor differences of bond distances and angles with respect to **1**. Likewise, the ^{31}P- and ^{15}N-NMR-spectroscopic properties of **2** were found to be quite similar to those of **1**, apart from characteristic differences in chemical shifts and coupling constants. Based on the strong activation of N$_2$, **2** could be converted to the hydrazido(2-) derivative **3** by protonation with HBAr^{F}, similar to **1**, rendering comparison to the analogous Mo-NNH$_2$ complex possible as well.
In order to obtain information about the electronic-structural properties of the tungsten and molybdenum pentaPod systems, electro- and spectroelectrochemical investigations were performed on **1** and **2**. Both dinitrogen complexes exhibit remarkably similar redox potentials. Moreover, two main systems can be detected in oxidation. For tungsten, the first system is found to be reversible and the second, being irreversible at low scan rates, gets more reversible at higher scan rates. By contrast, the first system is only partially reversible for the molybdenum complex and irreversible for the second system. The origin of these differences could be elucidated with spectroelectrochemistry: upon oxidation of **2**, a stable W^{I}N$_2^+$ complex is formed whereas for the molybdenum complex **1** loss of N$_2$ occurs, probably going along with a ligand exchange and formation of a THF-bound complex. For W, loss of N$_2$ only occurs upon further oxidation of the W^{I}N$_2^+$ complex.
In conclusion, the spectroelectrochemical studies as well as the voltammetric studies showed that both systems can regenerate the zerovalent dinitrogen complexes around the same potential. Furthermore, a stable tungsten dinitrogen complex is already formed at the level of a W(I) intermediate, exhibiting a fairly activated N$_2$ ligand with a ν_{NN} of 1951 cm^{-1} in solution. By contrast, the corresponding Mo(I) dinitrogen complex is thermally unstable. A theoretical mechanism evaluated for N$_2$-reduction of the molybdenum pentaPod system indicated that PCET to the Mo(N$_2$)-complex, generating a diazenido(-) intermediate, is energetically more favourable for a Mo(I)- than for a Mo(0)-species.[14] Based on the results presented here, the tungsten complex **2** would fit much better to such a scenario than its molybdenum analogue **1**. Nevertheless, NH$_3$ formation mediated by **2** is only slightly overstoichiometric. The reason(s) for this observation must therefore lie in some other stage of the catalytic cycle. Further investigation of this question is underway.

5. Experimental Section

All syntheses were performed under N$_2$ or Argon atmosphere using standard Schlenk line and glovebox techniques. The solvents were dried and freshly distilled under argon prior to use. [H(OEt$_2$)$_2$][Al(OC(CF$_3$)$_3$)$_4$] was received from the working group of I. Krossing in Freiburg i. Br. All other reagents were commercially available and were used as received. [WCl$_4$(PMePh$_2$)$_2$][31], [Mo(N$_2$)(P^{Me}$_2$PP^{Ph}$_2$)] (**1**)[13] and [Mo(NNH$_2$)(P^{Me}$_2$PP^{Ph}$_2$)][14] were prepared according to the literature. NMR spectra were recorded with a Bruker AVANCE III HD Pulse Fourier Transform spectrometer operating at frequencies of 400.13 MHz (^{1}H), 376.50 (^{19}F),

161.98 MHz (^{31}P), 128.38 (^{11}B), and 40.56 MHz (^{15}N). Referencing was performed either using the solvent residue signal (5.32 ppm for CD_2Cl_2, 3.58 ppm for thf-d_8 and 7.16 ppm for C_6D_6) or TMS (δ^1H = 0 ppm), $CFCl_3$ (δ^{19}F = 0 ppm), 85% H_3PO_4 (δ^{31}P = 0 ppm), BF_3 ((δ^{11}B = 0 ppm), and CH_3NO_2 (δ^{15}N = 0 ppm) serving as substitutive standards. IR spectra were recorded at RT on a Bruker Vertex70 FT-IR spectrometer using a broadband spectral range extension VERTEX FM for full mid and far IR in the range of 6.000-80 cm^{-1}.
Electrochemical studies were performed in a glovebox (Jacomex) (O_2 < 1 ppm, H_2O < 1 ppm) with a home-made 3-electrode cell (WE: Pt or glassy carbon, RE: Pt wire in a 1 mM Fc^+/Fc, 0.02 M THF/$NaBPh_4$ solution, CE : Pt). Ferrocene was added at the end of the experiments to determine the exact redox potential values. The potential of the cell was controlled by an AUTOLAB PGSTAT 100 (Metrohm) potentiostat monitored by the NOVA© software (Metrohm). The working electrodes were polished over a 1 µm alumina slurry with water, sonicated in H_2O (18.2 Ω·cm) and acetone, then dried with N_2 flush.
Thin layer IR spectroelectrochemistry was carried out with a previously described set-up consisting of a commercial IR Si ATR probe (Artphotonics), which can fit into a thin space created on the surface of a glassy carbon electrode.[32] The thin layer between the probe and the electrode allows fast (seconds) electrolysis, hence time-resolved monitoring of the electrochemical reaction. Detection of the IR signal (2 cm^{-1} resolution, one spectrum every 10 sec.) was obtained by using a FTIR optic-fiber-coupled spectrometer purchased from Arcoptix (FTMIR-FC-120-LN2).

Single crystal structure determination.
Data collection was performed using an Imaging Plate Diffraction System (IPDS-2) from Stoe&Cie with Mo-Kα radiation. A numerical absorption correction was performed using X-Red and X-Shape of the software package X-Area. The structures were solved with SHELXT[33] and structure refinement was performed against F^2 using SHELXL-2018[34] The C-H hydrogen atoms were positioned with idealized geometry (methyl H atoms allowed to rotate but not to tip) and were refined isotropic with Uiso (H) = 1.2 Ueq (C) (1.5 for methyl H atoms) using a riding model.
CCDC 2127859 (**2**) contains the supplementary crystallographic data for this paper. These data can be obtained free charge from the Cambridge Crystallographic Data Centre via http://www.ccdc.cam.ac.uk/data_request/cif.

[$WCl_3(\kappa^3$-$P^{Me}_2PP^{Ph}_2$)]
1.11 g (1.53 mmol) of [$WCl_4(PMePh_2)_2$] and 1.24 g (1.83 mmol) of $P^{Me}_2PP^{Ph}_2$ were dissolved in 50 ml toluene and stirred for 3 h at 70 °C. The mixture was filtrated and concentrated *in vacuo* to 5 ml and 10 ml of diethyl ether was added. The green precipitate was filtered and washed with 10 ml diethyl ether and 10 ml *n*-pentane. Drying in vacuo gave a dark green solid. Yield: 1.26 g (1.30 mmol, 85 %). Anal Calcd for $C_{39}H_{53}Cl_3P_5W$: C, 48.4; H, 5.52; Found: C, 48.9; H, 5.65. IR (300 K): ṽ = 3067 (w), 3051 (w), 2954 (sh), 2919 (m), 2867 (sh), 2801 (w), 1589 (m), 1568 (w), 1551 (vw), 1480 (m), 1455 (vw), 1430 (m), 1412 (w), 1381 (w), 1330 (vw), 1297 (w), 1279 (W), 1260 (vw), 1241 (w), 1182 (w), 1156 (w), 1119 (w), 1096 (m), 1069 (w), 1025 (w), 1000 (w), 945 (m), 917 (m), 880 (m), 843 (w), 805 (vw), 739 (s), 693(s), 639 (vw), 617 (w), 577 (vw), 543 (w), 508 (s), 479 (m), 442 (vw), 425 (w), 404 (vw), 362 (vw), 340 (sh), 323 (sh), 294 (s), 271 (vs), 252 (sh), 221 (vw), 208 (vw), 178 (w), 158 (w), 133 (m), 120 (w) cm^{-1}. Raman (300 K): ṽ = 6054 (m), 2982 (w), 2913 (s), 1586 (s), 1455 (vw), 1414 (w), 1306 (vw), 1210 (vw), 1186 (w), 1160 (w), 1100 (w), 1073 (vw), 1028 (m), 1000 (vs), 960 (w), 786 (w), 688 (w), 619 (w), 400 (vw), 328 (w), 258 (w), 150 (vw) cm^{-1}.

[$W(N_2)(P^{Me}_2PP^{Ph}_2)$] (**2**).
290 mg (300 mmol) of [$WCl_3(\kappa^3$-$P_2{}^{Me}PP_2{}^{Ph}$)] were dissolved in 20 ml THF and added to sodium amalgam prepared of 2 ml Hg and 200 mg of sodium. The reaction mixture was stirred for 16 h under an atmosphere of nitrogen. The supernatant red solution was transferred into another flask and the solvent was removed *in vacuo*. The residue was resolved in 10 ml of diethyl ether and filtered over neutral alumina. The orange solution was concentrated to dryness and shed with small amounts of cold n-pentane. Drying *in vacuo* gave an orange solid. Crystals suitable for X-ray single crystal diffraction were obtained by slow diffusion of *n*-pentane into a benzene-d_6 solution of **2**. Yield: Yield: 118 mg (133 µmol, 44 %). Anal Calcd for $C_{39}H_{53}N_2P_5W$: C, 52.7; H, 6.01; N, 3.15. Found: C, 53.4; H, 6.04; N, 2.30. The nitrogen value is too low because of the thermal instability of the product. $^{31}P\{^1H\}$ NMR (161.98 MHz, d_6-benzene, H_3PO_4, 300 K): δ = -4.8 (m, ^2J ($P_{AX'}$, $P_{A'X}$) = 85.7, ^2J (P_{AM}, $P_{A'M}$) = 11.2, ^2J (P_{AX}, $P_{A'X'}$) = -11.1, ^2J (P_A, $P_{A'}$) = 17.4 Hz, 2P, PPh_2, P_A/$P_{A'}$), -21.3 (tt, ^2J (P_{MX}, $P_{MX'}$) = 18.5 Hz, 1P, P_M), -35.8 (m, ^2J (P_X, $P_{X'}$) = 4.5 Hz, 2P, PMe_2, P_X/$P_{X'}$) ppm. IR (300 K): ṽ = 3139 (vw), 3069 (w), 3049 (w), 2994 (vw), 2959 (m), 2920 (sh), 2906 (m), 2855 (m), 2812 (sh), 1982 (w), 1901 (vs, ν(N-N)), 1805 (vw), 1750 (vw), 1585 (w), 1571 (w), 1481 (m), 1448 (w), 1431 (s), 1418 (sh), 1373 (w), 1328 (vw), 1293 (w), 1258 (s), 1218 (vw), 1184 (vw), 1153 (w), 1089 (s), 1072 (m), 1048 (m), 1025 (s), 970 (w), 925 (m), 905 (s), 875 (m), 832 (w), 798 (s), 737 (s), 693 (vs), 662 (s), 625 (s), 612 (s), 544 (vw), 506 (vs), 475 (m), 429 (w, ν(W-N)), 402 (s), 372 (vw), 345 (m), 313 (w), 290 (w), 263 (vw), 240 (m), 191 (vw) cm^{-1}. Raman (300 K): ṽ = 3053 (s), 2963 (w), 2912 (vs), 2888 (s), 2863 (sh), 1903 (s, ν(N-N)), 1587 (s), 1572 (w), 1451 (vw), 1434 (vw), 1418 (vw), 1405 (vw), 1297 (vw), 1274 (vw), 1186 (w), 1156 (w), 1093 (m), 1029 (m), 1001 (vs), 933 (vw), 910 (vw), 670 (w), 637 (vw), 618 (w), 505 (vw), 431 (w, ν(W-N)), 403 (vw), 364 (vw), 350 (vw), 315 (vw), 292 (vw), 257 (vw), 242 (w), 193 (w) cm^{-1}.
^{15}N-[$W(N_2)(P^{Me}_2PP^{Ph}_2)$] (**^{15}N-2**) was prepared in a similar fashion as **2** under a $^{15}N_2$ atmosphere and characterized by IR, Raman, ^{31}P- and ^{15}N NMR spectroscopy. $^{15}N\{^1H\}$ NMR (40.56 MHz, d_{10}-Et_2O, CH_3NO_2, 300 K): δ = -18.7 (d, $^1J_{NN}$ = 7.5 Hz, 1N, N_β), -48.4 (m, 1N, N_α) ppm. $^{31}P\{^1H\}$ NMR (161.98 MHz, d_6-benzene, H_3PO_4, 300 K): δ = -4.8 (m, ^2J ($P_{AA'}N_\alpha$) = 2.7 Hz, ^3J ($P_{AA'}N_\beta$) = 0.3 Hz, 2P, PPh_2, P_A/$P_{A'}$), -21.3 (ttdd, ^2J (P_M, N_α) = 13.9, ^3J (P_MN_β) = 1.6 Hz, 1P, P_M), -35.8(m, ^2J ($P_{XX'}N_\alpha$) = 2.6 Hz, ^3J ($P_{AA'}N_\beta$) = 0.7 Hz, 2P, PMe_2, P_X/$P_{X'}$) ppm. IR (300 K): ṽ = 1840 (vs, ν(N-N)), 421 (w, ν(W-N)) cm^{-1}. Raman (300 K): ṽ = 1840 (s, ν(N-N)), 419 (w, ν(W-N)) cm^{-1}.

[$W(NNH_2)(P^{Me}_2PP^{Ph}_2)$] ($BAr^F$)$_2$ (**3-BAr^F**).
A portion of 99.0 mg (97.9 µmol) of [$H(OEt_2)_2$][BAr^F] was dissolved in 0.4 mL of diethyl ether and added to 29 mg (32.6 µmol) of 3 in 0.6 mL of diethyl ether. After stirring for 5 min at room temperature the solvent was removed *in vacuo*, affording a light brown

solid in quantitative yield of nominal composition $[W(NNH_2)(P^{Me}{}_2PP^{Ph}{}_2)](BAr^F)_2 \cdot HBAr^F$. The high fluorine content precluded an elemental analysis. $^{31}P\{^1H\}$ NMR 161.98 MHz, d_{10}-Et_2O, H_3PO_4, 300 K): δ = -15.9 (m, ^2J ($P_{AX'}$, $P_{A'X}$) = 53.9, ^2J (P_{AM}, $P_{A'M}$) = 28.2, ^2J (P_{AX}, $P_{A'X'}$) = -12.2, ^2J (P_A, $P_{A'}$) = 16.1 Hz, 2P, PPh_2, $P_A/P_{A'}$), -45.8 (m, ^2J (P_{MX}, $P_{MX'}$) = 31.3, ^2J (P_X, $P_{X'}$) = 6.3 Hz, 2P, PMe_2, $P_X/P_{X'}$), -48.6 (tt, 1P, P_M) ppm. IR (300 K): $\tilde{\nu}$ = 3312 (w, ν(N-H)), 3076 (vw), 2960 (w), 2924 (m), 2853 (w), 1790 (vw), 1611 (m), 1443 (w), 1352 (s), 1272 (vs), 1159 (m), 1114 (vs), 1092 (sh), 998 (w), 934 (w), 918 (vw), 886 (s), 838 (s), 809 (m), 743 (m), 711 (s). 698 (w), 680 (s), 669 (s), 617 (vw), 609 (vw), 580 (w), 568 (vw), 516 (w), 507 (w), 488 (w), 449 (m), 403 (w), 392 (w), 380 (vw), 366 (m), 353 (sh), 331 (vw), 283 (w), 259 (w), 246 (vw), 210 (vw), 189 (vw), 151 (vw) cm^{-1}. Raman (300 K): $\tilde{\nu}$ = 3074 (w), 3023 (vw), 2960 8w), 2932 (m), 2906 (m), 2882 (sh), 2852 (w), 1611 (m), 1593 (s), 1523 (vw), 1464 (w), 1364 (s), 1107 (w), 1030 (w), 1003 (vs), 952 (w), 939 (vw), 914 (vw), 840 (vw), 801 (s), 745 (w), 704 (s), 689 (w), 675 (w), 617 (vw), 287 (w), 262 (w), 244 (vw), 235 (w), 183 (W), 159 (m) cm^{-1}.

^{15}N-$[W(NNH_2)(P^{Me}{}_2PP^{Ph}{}_2)](BAr^F)_2$ (**^{15}N-3-BAr^F**) was prepared in a similar fashion starting from ^{15}N-2 and characterized by IR, Raman, ^{31}P- and ^{15}N NMR spectroscopy. $^{15}N\{^1H\}$ NMR (40.56 MHz, d_{10}-Et_2O, CH_3NO_2, 300 K): δ = -48.4 (m, 1N, N_α), -237 (m, 1N, N_β) ppm. $^{31}P\{^1H\}$ NMR 161.98 MHz, d_{10}-Et_2O, H_3PO_4, 300 K): δ = -15.9 (m, ^2J ($P_{AA'}N_\alpha$) = 5.0 Hz, 2P, PPh_2, $P_A/P_{A'}$), -45.8 (m, ^2J ($P_{XX'}N_\alpha$) = 5.5 Hz, 2P, PMe_2, $P_X/P_{X'}$), -48.6 (ttdd, ^2J (P_M, N_α) = 20.4 Hz, ^3J (P_MN_β) = 6.6 Hz, 1P, PM) ppm. IR (300 K): $\tilde{\nu}$ = 3308 (w, ν(N-H)), 554 (w, ν(W-N)) cm^{-1}.

$[W(NNH_2)(P^{Me}{}_2PP^{Ph}{}_2)][Al(pftb)_4]_2$ (**3-Al(pftb)$_4$**) was prepared similar to **3-BAr^F** with $[H(OEt_2)_2][Al(OC(CF_3)_3)_4]$ as acid.

References

1 a) Y. Tanabe, Y. Nishibayashi, *Chem. Soc. Rev.* **2021**, *50*; b) M. J. Chalkley, M. W. Drover, J. C. Peters, *Chem. Rev.* **2020**, *120*, 5582; c) N. Stucke, B. M. Flöser, T. Weyrich, F. Tuczek, *Eur. J. Inorg. Chem.* **2018**, *2018*, 1337.

2 a) L. C. Seefeldt, Z.-Y. Yang, D. A. Lukoyanov, D. F. Harris, D. R. Dean, S. Raugei, B. M. Hoffman, *Chem. Rev.* **2020**, *120*, 5082; b) C. van Stappen, L. Decamps, G. E. Cutsail, R. Bjornsson, J. T. Henthorn, J. A. Birrell, S. DeBeer, *Chem. Rev.* **2020**, *120*, 5005; c) A. J. Jasniewski, C. C. Lee, M. W. Ribbe, Y. Hu, *Chem. Rev.* **2020**, *120*, 5107.

3 R. Schlögl, *Angew. Chem. Int. Ed.* **2003**, *42*, 2004.

4 a) M. D. Fryzuk, *Chem. Commun.* **2013**, *49*, 4866; b) A. D. Allen, C. V. Senoff, *Chem. Commun.* **1965**, *24*, 621.

5 a) J. Chatt, A. J. Pearman, R. L. Richards, *Nature* **1975**, *253*, 39; b) M. Hidai, K. Tominari, Y. Uchida, A. Misono, *Chem. Commun.* **1969**, 1392; c) M. Hidai, K. Tominari, Y. Uchida, *J. Am. Chem. Soc.* **1972**, *94*, 110.

6 C. J. Pickett, J. Talarmin, *Nature* **1985**, *317*, 652.

7 D. V. Yandulov, R. R. Schrock, *Science* **2003**, *301*, 76.

8 R. R. Schrock, *Acc. Chem. Res.* **2005**, *38*, 955.

9 a) K. Arashiba, Y. Miyake, Y. Nishibayashi, *Nat. Chem.* **2011**, *3*, 120; b) A. Eizawa, K. Arashiba, H. Tanaka, S. Kuriyama, Y. Matsuo, K. Nakajima, K. Yoshizawa, Y. Nishibayashi, *Nature Commun.* **2017**, *8*, 14874.

10 Y. Ashida, K. Arashiba, K. Nakajima, Y. Nishibayashi, *Nature* **2019**, *568*, 536.

11 K. Arashiba, K. Sasaki, S. Kuriyama, Y. Miyake, H. Nakanishi, Y. Nishibayashi, *Organometallics* **2012**, *31*, 2035.

12 D. V. Yandulov, R. R. Schrock, *Can. J. Chem.* **2005**, *83*, 341.

13 S. Hinrichsen, A. Kindjajev, S. Adomeit, J. Krahmer, C. Näther, F. Tuczek, *Inorg. Chem.* **2016**, *55*, 8712.

14 T. A. Engesser, A. Kindjajev, J. Junge, J. Krahmer, F. Tuczek, *Chem. Eur. J.* **2020**, *26*, 14807.

15 E. Carmona, A. Galindo, M. L. Poveda, R. D. Rogers, *Inorg. Chem.* **1985**, *24*, 4033.

16 S. L. Apps, A. J. P. White, P. W. Miller, N. J. Long, *Dalton Trans.* **2018**, *47*, 11386.

17 F. B. Ogilvie, J. M. Jenkins, J. G. Verkade, *J. Am. Chem. Soc.* **1970**, *92*, 1916.

18 a) A. Galindo, E. Gutierrez, A. Monge, M. Paneque, A. Pastor, P. J. Perez, R. D. Rogers, E. Carmona, *J. Chem. Soc. Dalton Trans.* **1995**, 3801; b) E. Carmona, J. M. Marin, M. L. Poveda, J. L. Atwood, R. D. Rogers, *J. Am. Chem. Soc.* **1983**, *105*, 3014.

19 J.-M. Savéant, *Elements of Molecular and Biomolecular Electrochemistry: An Electrochemical Approach to Electron Transfer Chemistry*, Wiley, Hoboken NJ, **2006**.

20 C. M. Elson, *Inorg. Chim. Acta* **1976**, *18*, 209.

21 C. J. Weiss, A. N. Groves, M. T. Mock, W. G. Dougherty, W. S. Kassel, M. L. Helm, D. L. DuBois, R. M. Bullock, *Dalton Trans.* **2012**, *41*, 4517.

22 D. V. Yandulov, R. R. Schrock, *Inorg. Chem.* **2005**, *44*, 1103.

23 A. Katayama, T. Ohta, Y. Wasada-Tsutsui, T. Inomata, T. Ozawa, T. Ogura, H. Masuda, *Angew. Chem. Int. Ed.* **2019**, *58*, 11279.

24 J. Chatt, H. Wasif, G. J. Leigh, H. Neukomm, C. J. Pickett, D. A. Rankin, *J. Chem. Soc. Chem. Comm.* **1980**, 1024.

25 J. J. Curley, T. R. Cook, S. Y. Reece, P. Müller, C. C. Cummins, *J. Am. Chem. Soc.* **2008**, *130*, 9394.

26 G. E. Greco, R. R. Schrock, *Inorg. Chem.* **2001**, *40*, 3861.

27 G. A. Silantyev, M. Förster, B. Schluschaß, J. Abbenseth, C. Würtele, C. Volkmann, M. C. Holthausen, S. Schneider, *Angew. Chem. Int. Ed.* **2017**, *56*, 5872.

28 M. W. Weatherburn, *Anal. Chem.* **1967**, *39*, 971.

29 C. J. Weiss, J. D. Egbert, S. Chen, M. L. Helm, R. M. Bullock, M. T. Mock, *Organometallics* **2014**, *33*, 2189.

30 K. H. Horn, N. Böres, N. Lehnert, K. Mersmann, C. Näther, G. Peters, F. Tuczek, *Inorg. Chem.* **2005**, *44*, 3016.

31 F. Basolo, R. J. Angelici (Eds.) *Inorganic syntheses*, *Vol. 28*, Wiley, New York, **1990**.

32 C. Garcia Bellido, L. Álvarez-Miguel, D. Miguel, N. Lalaoui, N. Cabon, F. Gloaguen, N. Le Poul, *ChemElectroChem* **2021**, *8*, 1899.

33 G. M. Sheldrick, *Acta Cryst.* **2015**, *A71*, 3.

34 G. M. Sheldrick, *Acta Cryst.* **2015**, *C71*, 3.

Conflicts of interest

The authors declare no conflict of interest

Acknowledgements

The authors gratefully acknowledge the SEA-EU program supported by Agence Nationale de la recherche (ANR-19-GURE-0001), PHC Procope Campus France (46652ZL) and Programm des Projektbezogenen Personenaustauschs Frankreich (PROCOPE) 2021-2023 (Deutscher Akademischer Austauschdienst, Projekt-Kennziffer 57560918) for funding. The authors thank Prof. Ingo Krossing for providing us with $[H(OEt_2)_2][Al(OC(CF_3)_3)_4]$.